CONODONTS: Investigative Techniques and Applications

Editor:
RONALD L. AUSTIN, B.Sc., Ph.D.
Senior Lecturer
University of Southampton

Published by
ELLIS HORWOOD LIMITED
Publishers · Chichester
for
THE BRITISH MICROPALAEONTOLOGICAL SOCIETY

16

Conodont chemostratigraphy across the Cambrian–Ordovician boundary: western USA and southeast China

J. Wright, J. F. Miller and W. T. Holser

The trace-element composition of biogenic apatite contains a detailed record of perturbations of sea-water chemistry that is useful for regional and intercontinental correlation; such correlations are referred to as chemostratigraphy. Detailed studies of conodont and some inarticulate brachiopod apatite from sections spanning the Cambrian–Ordovician boundary show that strata can be correlated by secular variations of trace elements. These strata consist of marine carbonates deposited in different tectonic settings: the Texas strata were deposited in a marginal cratonic sea, the Oklahoma strata in an aulacogen and the Utah strata on a carbonate platform. The strata in southeast China were deposited in slightly deeper water on a continental shelf. Precise biostratigraphic correlation is controlled by important conodont and trilobite lineages and by well-defined eustatic events. The biostratigraphic horizons are used as the basis for correlation of the chemical signatures. Chemical data from conodont and inarticulate brachiopod samples in the western USA show excellent correlation of secular variations of the cerium anomaly in rare-earth element patterns. A metal-rich zone occurs a the base of the Late Cambrian *Cordylodu proavus* conodont zone and coincides with th first occurrence of *Eurekia apopsis* trilobites i western USA sections. A similar geochemica signal is recognized in the section from Chin and was used to predict the correlative horizo in China.

16.1 INTRODUCTION

Previous work has shown that carbonate apatit of conodonts, inarticulate brachiopods and fis all retain a greatly enriched but unfractionate geochemical signature of the sea-water in whic the skeletal material was deposited (Wright an Holser, 1981; Wright-Clark, 1982; Wrigh *et al.*, 1984; Shaw and Wasserburg, 1985 Keto and Jacobson, 1985; Elderfield an Pagett, in press; Staudigel *et al.*, in press). W report the first detailed chemostratigraphi study of trace-element variations through a tim interval encompassing the Cambrian–Ordovi cian boundary. The strata investigated consis of well-exposed marine carbonates deposited i

different tectonic settings in the western USA (Miller *et al.*, 1982) and southeast China (Lu and Lin, 1983). Fig. 16.1 shows the locations of sections on a reconstruction of plate positions during Late Cambrian times (Scotese *et al.*, 1979). The Lange Ranch section is in the Llano Region of Texas and was deposited near the oceanic margin of a shallow cratonic sea. The Chandler Creek section in the Wichita Mountains of Oklahoma was deposited in an aulacogen. The Lava Dam sections in the House Range, Utah, were deposited on a carbonate platform. The Dadoushan section in western Zhejiang Province, China, represents relatively deep-water deposition on a continental shelf. Table 16.1 lists the intervals at which each section was sampled and includes the stratigraphic position of each sample as measured from the base of Miller's sections.

The present chapter deals with a portion of a broader study of the trace-element geochemistry of Palaeozoic to Recent biogenic apatite. The Cambrian–Ordovician boundary interval was chosen for detailed study for two reasons. First, Miller (1984) proposed that two worldwide eustatic events (possibly related to glaciation in Gondwanaland) strongly affected the evolution of contemporary conodonts and other marine invertebrates during this boundary interval. It seemed likely that these eustatic events might also have produced geochemical changes in seawater that were recorded in conodonts and other skeletal apatite. Second, the IUGS International Working Group on the Cambrian–Ordovician Boundary is in the process of standardizing the base of the Ordovician System by considering the definition of a boundary point in a stratotype section. Geochemical research that might shed new light on problems of correlation and on environmental interpretations is therefore particularly timely.

16.2 SAMPLE PREPARATION

In the present study we used a composite of all taxa of either conodont elements or inarticulate brachiopod shells recovered from each sample.

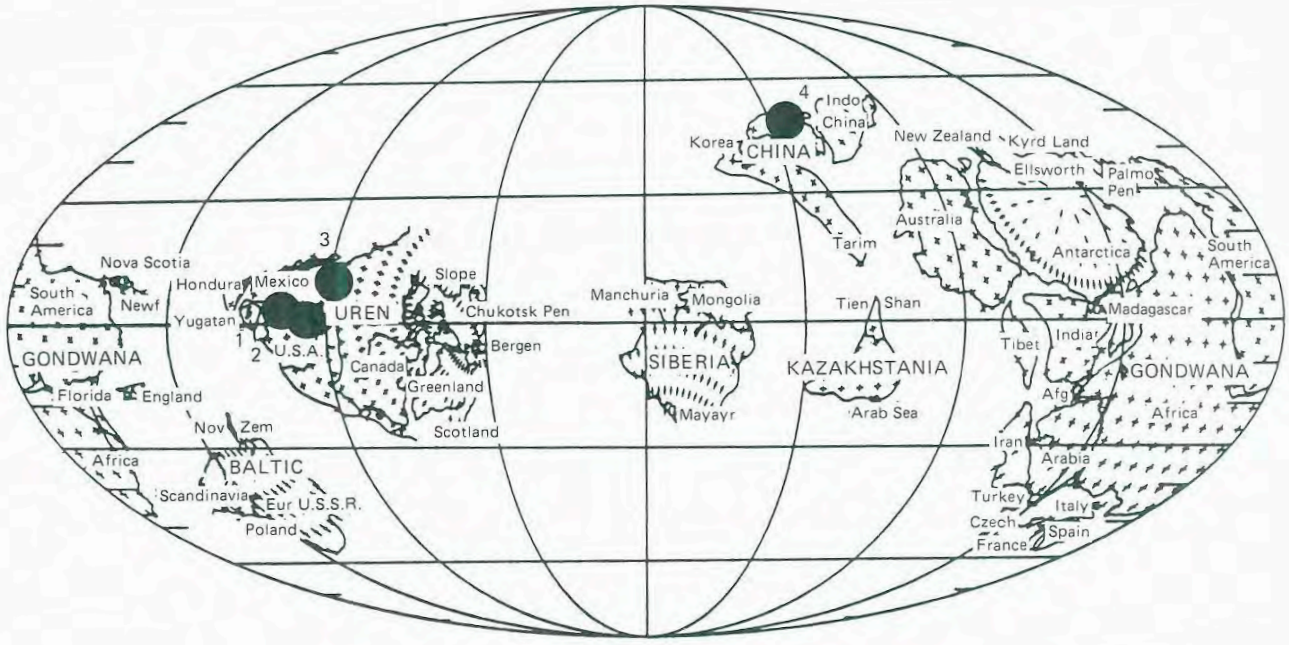

Fig. 16.1 — Palaeogeographical reconstruction of continental positions for middle Late Cambrian (Franconian Age). Mollweide equal-area projection. Sample locations are as follows: 1, Texas; 2, Oklahoma; 3, Utah; 4, China. (After Scotese *et al.* (1979).)

Table 16.1 — Locations and chronostratigraphic units from which samples were collected.

Sample	System	Series or stage	Location	Formation
JW3-9Br	Ordovician	'Ibexian' Series*	Lange Ranch, Texas	Tanyard Formation 1517 ft
JW3-8Br	Ordovician	'Ibexian' Series*	Lange Ranch, Texas	Wilberns Formation 1512 ft
JW3-5MEI-WU;5NS-WU; 5Br-NASA; 5MEI-NASA; 5NS-NASA	Ordovician	'Ibexian' Series*	Lange Ranch, Texas	1497 ft
JW3-4Br-WU; 4Br-NASA	Ordovician	'Ibexian' Series*	Lange Ranch, Texas	1492 ft
JW3-3Br	Ordovician	'Ibexian' Series*	Lange Ranch, Texas	1487 ft
JW3-24NS-WU; 24Br-NASA; 24NS-NASA; 24MEI-NASA; 24MEI/cl-NASA	Ordovician	'Ibexian' Series*	Lange Ranch, Texas	1472 ft
JW3-23NS-WU; 23NS-WU†; 23Br-NASA; 23MEI-NASA	Ordovician	'Ibexian' Series*	Lange Ranch, Texas	1457 ft
JW3-17Br-WU; 17Br-NASA	Ordovician	'Ibexian' Series*	Lange Ranch, Texas	1412 ft
JW3-17A-Br-WU	Ordovician	'Ibexian' Series*	Lange Ranch, Texas	1411.5 ft
JW2-9.5A-Br; 9.5B-Br‡	Cambrian	Trempealeauan Stage	Lange Ranch, Texas	Wilberns Formation, 1400.5 ft
JW2-9Br; 9Br†	Cambrian	Trempealeauan Stage	Lange Ranch, Texas	>1400 ft
JW2-8Br-WU; 8Br-WU†; 8Br-NASA	Cambrian	Trempealeauan Stage	Lange Ranch, Texas	<1400 ft
JW2-25Br-NASA	Cambrian	Trempealeauan Stage	Lange Ranch, Texas	1132 ft
JW3-46Br	Ordovician	'Ibexian' Series*	Chandler Creek, Oklahoma	Signal Mountain Limestone, 1910 ft
JW3-34Br-WU; 34Br-WU†; 34Br-NASA; 34NS-NASA; 34MEI-NASA	Ordovician	'Ibexian' Series*	Chandler Creek, Oklahoma	1687 ft
JW3-31Br	Ordovician	'Ibexian' Series*	Chandler Creek, Oklahoma	1529 ft
JW3-29Br	Ordovician	'Ibexian' Series*	Chandler Creek, Oklahoma	1512 ft
JW3-28Br	Ordovician	'Ibexian' Series*	Chandler Creek, Oklahoma	1508 ft
JW3-27Br	Ordovician	'Ibexian' Series*	Chandler Creek, Oklahoma	1500 ft
JW3-26Br	Ordovician	'Ibexian' Series*	Chandler Creek, Oklahoma	1497 ft
JW3-25Br; 25Br†	Cambrian	Trempealeauan Stage	Chandler Creek, Oklahoma	1490 ft
JW2-37Br	Cambrian	Trempealeauan Stag	Chandler Creek, Oklahoma	1427 ft
JW3-75Br‡	Ordovician	'Ibexian' Series*	House Range, Utah	Fillmore Formation, 2291 ft
JW3-73Br	Ordovician	'Ibexian' Series*	House Range, Utah	2271 ft
JW3-71Br	Ordovician	'Ibexian' Series*	House Range, Utah	House Limestone, 2246 ft
JW3-67Br	Ordovician	'Ibexian' Series*	House Range, Utah	2150 ft
JW3-65Br	Ordovician	'Ibexian' Series*	House Range, Utah	2125 ft
JW3-64Br	Ordovician	'Ibexian' Series*	House Range, Utah	2109 ft
JW3-58Br	Ordovician	'Ibexian' Series*	House Range, Utah	2101 ft
JW3-57Br; 57Br†	Ordovician	'Ibexian' Series*	House Range, Utah	2080 ft
JW3-59Br	Ordovician	'Ibexian' Series*	House Range, Utah	2048 ft
JW3-54Br	Ordovician	'Ibexian' Series*	House Range, Utah	1710 ft
JW3-52Br	Ordovician	'Ibexian' Series*	House Range, Utah	Notch Peak Formation, 1601 ft
JW3-50Br‡	Ordovician	'Ibexian' Series*	House Range, Utah	1592 ft
JW3(2)-55Br	Cambrian	Trempealeauan Stage	House Range, Utah	1583 ft 4 in
JW2-54A-Br; 54B-Br; 54B-Br†	Cambrian	Trempealeauan Stage	House Range, Utah	1582 ft 8 in
JW2-45Br‡	Cambrian	Trempealeauan Stage	House Range, Utah	Orr Formation, 287 ft
JW2-40Br‡	Cambrian	Trempealeauan Stage	House Range, Utah	96 ft
JW3-101Br; 101Br†	Ordovician	Lower Ordovician Series	Dadoushan, southeast China	Yinchupu Formation, 269 ft
JW3-100Br	Ordovician	Lower Ordovician Series	Dadoushan, southeast China	197 ft
JW2-105Br; 105Br†	Cambrian	Upper Cambrian Series	Dadoushan, southeast China	Siyangshan Formation, 184 ft
JW2-104A-Br; 104A-Br†;104B-Br‡	Cambrian	Upper Cambrian Series	Dadoushan, southeast China	164 ft
JW2-103Br; 103Br†	Cambrian	Upper Cambrian Series	Dadoushan, southeast China	151 ft
JW2-102Br;2-102Br†	Cambrian	Upper Cambrian Series	Dadoushan, southeast China	144 ft
JW2-101Br‡	Cambrian	Upper Cambrian Series	Dadoushan, southeast China	133 ft
JW2-100Br; 100Br†	Cambrian	Upper Cambrian Series	Dadoushan, southeast China	125 ft

† Weight corrected to average CaO content of 52 wt. %.

‡ Inarticulate brachiopod sample.

* Ibexian was introduced as a series name for the Lower Ordovician in North America by Hintze (1982). We place the name, Ibexian, in quotation marks because it may not be possible to use it as a series name. Ibexian may be preoccupied by previous use as the Ibex Substage of LeMone (1975) or as the Ibex Member of the Ely Springs Dolostone of Budge and Sheehan (1980).

The use of composite samples minimizes metabolic effects and gives an average of the seawater environment in which the organisms were deposited. The carbonate matrix of samples was removed by dissolution in 10% acetic acid. Fossil apatite was further concentrated in the heavy liquid tetrabromoethane. Tests for chemical contamination by acetic acid or tetrabromoethane (Wright, 1985; Shaw, 1984) show that heavy liquids may remove part of the trace elements present but do not cause fractionation. Fig. 16.2 compares the rare-earth element patterns of samples of conodonts prepared three ways: hand picked without heavy-liquid concentration, concentrated with tetrabromoethane, or concentrated with methylene iodide. Use of either heavy liquid reduces the absolute concentration of rare-earth elements, but the rare-earth element patterns look the same, i.e. no fractionation occurs. Isotopic tracer studies of conodonts separated mechanically compared with those separated chemically with acetic acid also show removal or exchange of rare earths, but no fractionation (Shaw,. 1984). Comparison of bromine contents of samples analysed with and without the use of tetrabromoethane (Table 16.2) indicate that bromine is added during heavy-liquid separation and does not occur naturally in the fossil apatite. It is advisable to run similar tests for chemical contamination when using other reagents, e.g. sodium hypochlorite, which also might affect elemental concentrations.

After this two-step separation process, conodont elements or inarticulate brachiopod shells were hand picked from the heavy fraction of the insoluble residue using pure alcohol as a wetting agent. Each sample of fossil material was cleaned ultrasonically in pure alcohol to remove any adhering material, particularly clays and iron minerals. Each sample was then filtered with a millipore system and whole fossils or fragments were hand picked again to ensure that extraneous material was not included in the final portion to be analysed. Samples were placed in ultrapure quartz glass tubes and sealed by fusing the glass in a flame. Sample weights were determined by weight difference of the empty and filled quartz tubes prior to sealing. The sensitivity of the balance for each weight is ± 0.01 mg. For very small samples, e.g. less than 0.20 mg, this may be a significant source of error. The analytical data for very small conodont samples have been normalized to a nominal CaO concentration for apatite of 52 ± 4 wt. % (Pietzner *et al.*, 1968; Deer *et al.*, 1966). These normalized values are listed in Table 16.2 after the set of values calculated using the measured weight. Normalization to a nominal CaO concentration does not change the shape of the rare-earth element pattern or the value of the cerium anomaly.

16.3 ANALYTICAL PROCEDURES

Instrumental neutron activation analysis was used to determine trace-element contents of samples. Instrumental neutron activation analysis is a quantitative application of γ-ray spectroscopy. It is a non-destructive and highly sensitive technique by which concentrations of many elements may be determined simultaneously. A general description of this technique has been given by Laul (1979). Modifications to standard procedures which facilitate analysis of small microfossil samples include the use of high-purity quartz tubes, high neutron flux ($(1–5) \times 10^{18}$ neutrons cm^{-1}) and long counting times (8–12 h). Samples were analysed at either the Johnson Space Center, National Aeronautics and Space Administration, Houston, Texas, or at Washington University, St. Louis, Missouri, using the procedures of Jacobs *et al.* (1977). Recent modifications at Washington University include the use of the TEABAGS computer program (Lindstrom and Korotev, 1982) and new fly-ash standards (Korotev, in press). Interlaboratory bias was negligible between the two laboratories. Analytical uncertainties were lower at Washington University because of a higher neutron flux and longer counting times. Fig. 16.2 illustrates the consistency of analyses for splits of the same sample analysed at each laboratory. Small variations in

neodymium between the laboratories result from the differences in counting times and neutron fluxes.

Trace-element data for Cambrian–Ordovician boundary samples are given in Table 16.2. All trace elements are in parts per million (pp
except gold which is in parts per billion (pp
At the range and level of elemental concentrations reported here, the 1σ (one standard deviation) error based on counting statistic

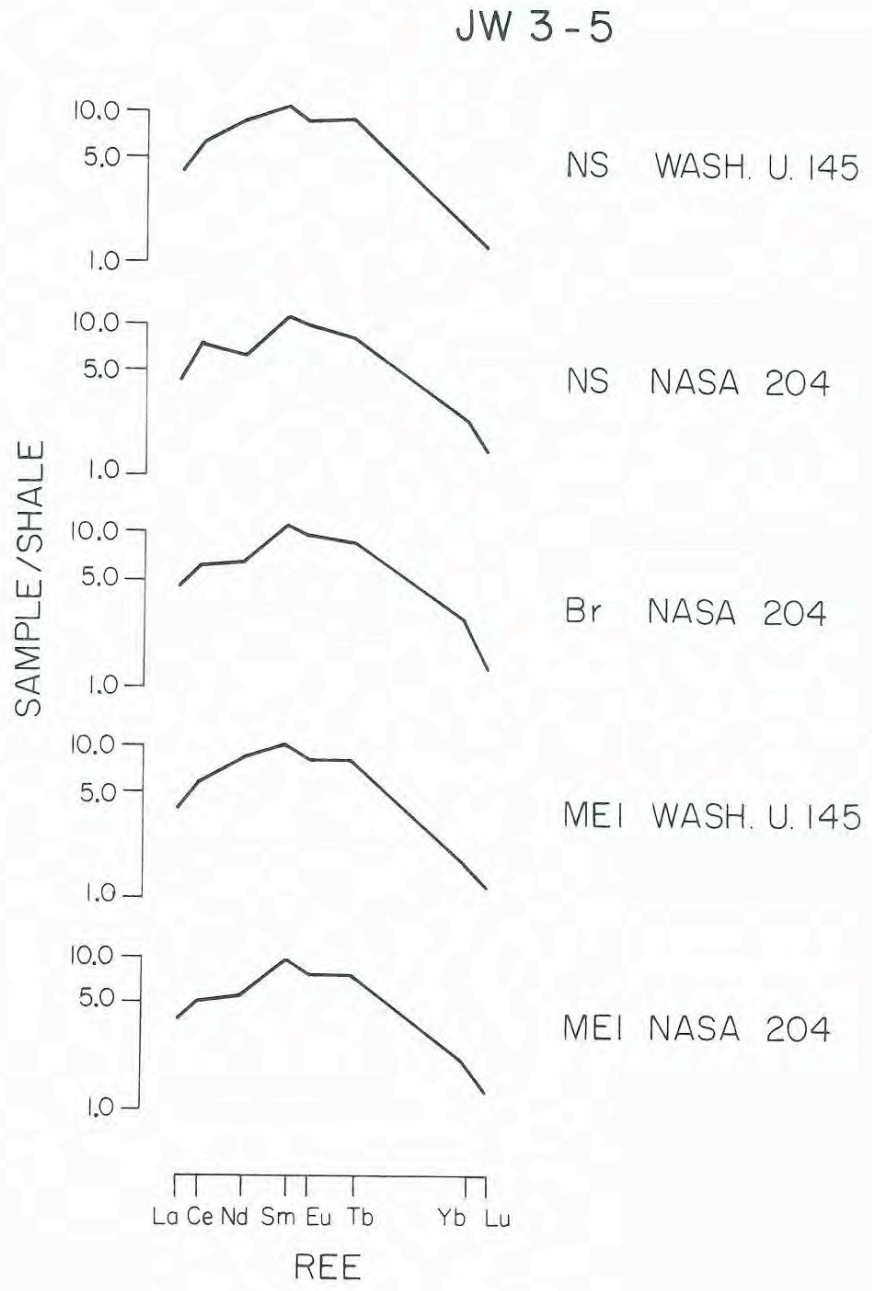

Fig. 16.2 — Comparison of rare-earth element patterns of samples: Br, separated with tetrabromoethane; MEI, separated with methylene iodide; NS, not separated with heavy liquid. They also show the variation in rare-earth element analyses between different instrumental neutron activation analysis laboratories: WASH U, Washington University, St. Louis, Missouri; NASA, National Aeronautics and Space Administration, Johnson Space Center, Houston, Texas. Concentrations normalized to shales are indicated on a logarithmic scale on the vertical axis. See text for further explanation.

Table 16.2 — Chemical data on conodonts from Cambrian–Ordovician boundary sections.

Texas	JW3-9Br	JW3-8Br	JW3-5MEI-WU	JW3-5NS-WU	JW3-5Br-NASA	JW3-5MEI-NASA
Trace elements						
Sc	6	0.4	0.9	1.2	0.8	0.7
Cr	66	220	69	70	13	12
Co	0.7	1	0.5	0.6	1.1	0.8
Ni	230	660	260	210	ND	100±60
Zn	100	56	65	68	38	32
As	ND	ND	ND	ND	ND	ND
Br	27	12	3	3	0.5	ND
Sr	9800	7000	6000	6400	5600	4600
Sb	0.04±0.08	0.01±0.28	0.2±0.1	0.1±0.1	ND	ND
La	200	100	130	130	150	130
Ce	620	270	420	460	450	380
Nd	590	190	280	300	220	190
Sm	130	43	57	62	65	54
Eu	18	7	10	11	12	10
Tb	13	3.7	6.9	7.7	7.6	6.5
Yb	7	3	5.1	5.1	8.5	6.4
Lu	0.9	0.2±0.1	0.5	0.6	0.6	0.6
Au	8±6	8±11	−3±5	4±4	6.9	5.6
Th	77	47	47	51	61	37
U	9.4	11	9.5	9.8	12	11
Mass (mg)	1.01	0.14	0.46	0.29	1.10	0.98

Table 16.2 — *continued.*

Texas	JW3-5NS-NASA	JW3-4Br-WU	JW3-4Br-NASA	JW3-3Br	JW3-24NS-WU	JW3-24Br-NASA
Trace elements						
Sc	1	2.5	3.2	0.31	4.7	2.9
Cr	23	17	24	110	67	ND
Co	2	0.3	1.4	0.7	0.5	1.4
Ni	ND	50±40	ND	350	210	NA
Zn	41	63	26	51	56	70
As	ND	ND	ND	ND	ND	NA
Br	ND	34	7.3	8.8	3.8	0.6
Sr	4200	5300	4700	5900	19100	6500
Sb	ND	0.01±0.1	ND	0.1±0.1	0.0±0.1	ND
La	130	150	160	60	180	160
Ce	550	530	600	180	540	480
Nd	210	350	350	120	370	180
Sm	63	74	84	24	65	120
Eu	12	12	15	4.2	10	9.5
Tb	7.1	8.5	9.7	2.8	7.5	6.3
Yb	7.3	6.2	8.5	1.7	5.8	5.9
Lu	0.6	0.7	0.8	0.2	0.7	0.5
Au	6.6	5±5	5.5	2±3	7±6	ND
Th	53	59	63	22	65	35
U	11.	8.5	9	7.7	12	13
Mass (mg)	0.55	0.82	0.95	0.44	0.42	0.94

Texas	JW3-24NS-NASA	JW3-24MEI-NASA	JW3-24MEI/cl-NASA	JW3-23NS-WU	JW3-23NS-WU*	JW3-23Br-NASA
Trace elements						
Sc	4.3	2.5	1.8	7.2	5.9	9.2
Cr	ND	ND	ND	78	64	55
Co	2	ND	2.4	1.4	1.2	3.1
Ni	NA	NA	NA	290	240	ND
Zn	61	120	140	90	74	ND
As	NA	NA	NA	ND	ND	ND
Br	ND	ND	0.2±0.1	ND	ND	6.7
Sr	5100	5700	4900	9000	7400	10100
Sb	ND	ND	ND	0.3±0.3	0.2±0.3	ND
La	200	170	110	260	210	250
Ce	650	470	390	880	730	1020
Nd	260	200	180	760	630	650
Sm	140	110	74	140	120	140
Eu	12	10	7.6	18	15	18
Tb	9.3	6.9	5.3	13	11	16
Yb	9.3	8.1	7.9	9.3	7.7	15
Lu	0.7	0.6	0.6	0.9	0.8	1.4
Au	ND	ND	ND	10±20	8±15	8.3
Th	58	23	30	93	76	106
U	14	16	13	11	8.9	20
Mass (mg)	0.60	0.55	0.23	0.15	0.12	0.20

Table 16.2 — *continued.*

Texas	JW3-23MEI-NASA	JW3-17Br-WU	JW3-17Br-NASA	JW3-17A-BR	JW2-9.5A-Br	JW2-9.5B-Br
Trace elements						
Sc	6.9	0.6	0.9	1.1	5.3	1.6
Cr	28	2.3	24	2±1	36	32
Co	1.6	0.5	2±1	0.7	2.3	0.8
Ni	120±70	20±10	ND	10±30	170	190
Zn	60	73	240	77	180	86
As	ND	ND	ND	3±2	8.6	ND
Br	1.2	18	1.2	2.7	4.2	ND
Sr	9100	5800	4200	5400	4700	2000
Sb	ND	0.06±0.03	ND	0.06±0.04	0.5±0.3	0.3±0.2
La	220	78	87	140	280	530
Ce	700	230	290	440	1290	1920
Nd	440	150	190	300	900	1430
Sm	120	32	37	65	180	250
Eu	16	5.1	7.1	10	31	40
Tb	9.9	3.7	5.2	7.5	21	30
Yb	11	2.5	3.5	4.4	11	15
Lu	1	0.3	0.7	0.5	1.4	1.7
Au	4.5	3±3	1.9	1±4	14±8	20±10
Th	59	14	15	18	50	10
U	9.8	5	7.6	6.2	18	41
Mass (mg)	0.78	1.08	0.53	0.81	0.21	0.51

Table 16.2 — *continued.*

Texas	JW2-9Br	JW2-9Br*	JW2-8Br-WU	JW2-8Br-WU*	JW2-8Br-NASA	JW2-25Br
Trace elements						
Sc	4.8	3.6	5.6	4.6	4.3	18
Cr	340	260	63	52	41	77
Co	4.3	3.2	7.4	6.1	12	31
Ni	1130	840	210	170	ND	ND
Zn	220	160	190	160	110	130
As	ND	ND	ND	ND	50±30	ND
Br	240	180	530	430	1.4	32
Sr	5100	3800	5200	4300	4000	2100
Sb	0.9	0.7	0.3±0.4	0.3±0.4	1.1±0.6	ND
La	580	430	260	230	230	410
Ce	2350	1740	960	790	1030	1930
Nd	1520	1130	640	530	270	860
Sm	330	240	130	110	130	220
Eu	51	38	20	17	24	44
Tb	39	29	14	12	14	28
Yb	25	18	7.8	6.4	12	24
Lu	3	2.2	0.8	0.7	0.9	2.3
Au	20±30	10±30	9±18	7±18	18	10
Th	140	110	26	21	33	81
U	22	16	13	11	11	25
Mass (mg)	0.05	0.04	0.11	0.09	0.33	0.20

Table 16.2 — *continued.*

Oklahoma	JW3-46Br	JW3-34Br-WU	JW3-34Br-WU*	JW3-34Br-NASA	JW3-34NS-NASA	JW3-34MEI-NASA
Trace elements						
Sc	0.4	2.7	3.3	2.3	5	1.6
Cr	17	24	29	NA	NA	NA
Co	0.4	0.5	0.5	1.8	26	18
Ni	40±50	50±90	60±90	NA	NA	NA
Zn	32	80	97	60	190	90
As	ND	ND	ND	NA	NA	NA
Br	12	24	29	0.7	ND	ND
Sr	5900	12000	14500	3500	3600	3300
Sb	0.0±0.2	0.4±0.8	0.5±0.8	ND	ND	ND
La	37	98	120	100	210	92
Ce	110	290	350	270	490	230
Nd	74	160	190	180	ND	ND
Sm	15	32	39	47	38	19
Eu	2.4	4.9	5.9	6.7	13	4.4
Tb	1.5	2.2	2.7	2.8	5.1	2.6
Yb	0.6	1.3	1.6	3.2	ND	ND
Lu	0.06±0.03	0.3	0.3	ND	ND	ND
Au	6±5	ND	ND	ND	ND	ND
Th	17	11	13	10	29	24
U	4.2	3.0	3.6	ND	ND	ND
Mass (mg)	0.73	0.17	0.21	0.46	0.23	0.45

Table 16.2 — *continued.*

Oklahoma	JW3-31Br	JW3-29Br	JW3-28Br	JW3-27Br	JW3-26Br	JW3-25Br
Trace elements						
Sc	0.4	1.2	0.7	0.5	2.1	2.7
Cr	5.4	11	7	0.5±3.4	6	13
Co	0.4	0.9	1.6	0.7	1	1.2
Ni	30±40	50±30	30±90	10±70	−30±70	0±120
Zn	79	64	69	90	65	80
As	ND	ND	10	ND	ND	ND
Br	10	14	27	12	17	53
Sr	5500	4900	5400	5300	4300	3700
Sb	0.1±0.1	0.1±0.1	0.5	0.02±0.35	0.2±0.3	0.3±0.7
La	26	91	66	38	84	160
Ce	98	380	220	93	250	860
Nd	65	190	110	59	150	610
Sm	12	33	20	10	26	110
Eu	1.8	5.6	3.5	1.8	4.3	19
Tb	0.9	3.1	1.6	0.7	2.5	10
Yb	0.5	1.7	0.5	0.3±0.2	1.1	2.8
Lu	0.04±0.04	0.2	0.06±0.04	0.1±0.1	0.2±0.1	0.3
Au	ND	−1±3	ND	ND	1±4	10±10
Th	11	34	13	15	32	38
U	2.1	3.5	2	1.4±0.9	3.8	6
Mass (mg)	1.07	0.77	0.35	0.35	0.51	0.17

Table 16.2 — *continued.*

Oklahoma	JW3-25Br*	JW2-37Br	Utah	JW3-75Br	JW3-73Br	JW3-71Br
Trace elements						
Sc	3.1	2.1		1.5	0.1	0.4
Cr	15	13		13	15	19
Co	1.4	0.8		1.7	0.5	1.4
Ni	0±100	30±100		10±30	56	30±70
Zn	92	100		61	39	61
As	ND	ND		ND	ND	6±9
Br	61	20		15	12	36
Sr	4300	6000		1600	18400	10700
Sb	0.4±0.7	0.4±0.9		0.1±0.1	0.07±0.10	0.1±0.3
La	190	55		140	42	47
Ce	1000	220		290	100	86
Nd	700	190		170	59	52
Sm	130	37		28	9.8	9.6
Eu	22	6.2		5.6	2	1.7
Tb	12	2.4		3.5	1	1.2
Yb	3.2	1.0		2.7	0.3±0.2	0.7
Lu	0.4	0.2±0.1		0.3	0.05±0.03	0.1±0.1
Au	20±10	ND		−1±5	ND	ND
Th	44	27		24	8.9	12
U	7	3.2		4.8	0.2±0.7	5.8
Mass (mg)	0.20	0.12		1.80	0.61	0.45

Table 16.2 — *continued.*

Utah	JW3-67Br	JW3-65Br	JW3-64Br	JW3-58Br	JW3-57Br	JW3-57Br*
Trace elements						
Sc	7	0.2	0.09	0.5	0.5	0.6
Cr	21	46	28	18	7±5	9±5
Co	2.9	0.6	0.2±0.1	0.5	0.8	1.1
Ni	50±130	140	71	30±20	10±70	20±70
Zn	79	ND	ND	65	90	120
As	ND	ND	ND	ND	ND	ND
Br	23	4	4.3	12	15	19
Sr	7200	10100	11500	9200	9300	12100
Sb	0.2±0.4	0.05±0.08	0.01±0.10	0.03±0.05	0.9±0.8	1.2±0.8
La	97	36	18	55	45	59
Ce	220	85	42	150	110	150
Nd	130	46	22	99	50	65
Sm	20	7.9	4	18	12	15
Eu	4	1.6	0.8	3.1	2.5	3.3
Tb	3.3	0.9	0.5	2.3	1.9	2.5
Yb	2.2	0.8	0.3	1.3	0.7	0.9
Lu	0.6	0.08	0.02±0.03	0.1	0.07±0.06	0.09±0.06
Au	ND	ND	ND	3±4	ND	ND
Th	9.5	3.8	1.8	13	8.7	11
U	1.5	1.3	1.1	1.8	5.9	7.7
Mass (mg)	0.27	0.97	0.89	0.97	0.18	0.23

Table 16.2 — *continued.*

Utah	JW3-59Br	JW3-54Br	JW3-52Br	JW3-50Br	JW2-55Br	JW2-54A-Br
Trace elements						
Sc	0.4	0.4	0.09	0.3	0.6	1.1
Cr	2±2	12	15	6.1	21	160
Co	2.3	1.3	0.7	3.7	1.4	2.5
Ni	0±60	0±60	40±20	−9±40	60	460
Zn	84	47	ND	ND	29	50
As	ND	11	5.3	37	12	53
Br	49	8.8	5.6	39	67	67
Sr	7100	8700	4900	3200	2900	2300
Sb	0.1±0.2	0.09±0.27	0.02±0.09	0.3	0.06±0.06	0.1±0.1
La	71	45	23	130	150	300
Ce	160	77	55	240	360	560
Nd	100	43	34	160	220	370
Sm	16	6.8	6.2	28	39	92
Eu	3.3	1.3	1.1	7.9	6.8	13
Tb	1.9	0.7	0.6	3.0	4.1	8.4
Yb	1.0	0.5	0.2±0.1	1.0	2.4	6
Lu	0.2	0.08	ND	0.2	0.2	0.7
Au	2±5	ND	ND	5±6	3±5	7±4
Th	2.4	8.8	8.3	7.1	54	21
U	2.1	1.1	0.7±0.4	5.7	5.3	19
Mass (mg)	0.74	0.49	0.99	0.44	0.69	0.63

Table 16.2 — *continued.*

Utah	JW2-54B-Br	JW2-54B-Br*	JW2-45Br	JW2-40Br	China	JW3-101Br
Trace elements						
Sc	14	10	0.5	0.4		0.7
Cr	103	71	10	4		38
Co	6.2	4.3	1.4	2±1		2.3
Ni	200±100	160±90	20±30	30±30		50±100
Zn	150	100	46	76		80
As	66	46	ND	ND		ND
Br	99	69	12	4±3		7.9
Sr	5000	3500	2400	1200		2700
Sb	0.7	0.5	0.01±0.05	0.00±0.06		0.6
La	330	230	210	170		73
Ce	670	480	460	360		180
Nd	520	360	300	260		190
Sm	96	67	50	39		40
Eu	18	13	8.6	10		7.2
Tb	10	7.2	5	4.9		4.5
Yb	5.2	3.6	2.6	1.8		1.3
Lu	0.8	0.6	0.3	0.3		0.2±0.1
Au	87	60	8±7	3.5		16±8
Th	52	36	17	8.2		23
U	14	9.5	7.3	9.3		1.5
Mass (mg)	0.05	0.04	1.97	0.92		0.08

Table 16.2 — *continued.*

China	JW3-101Br*	JW3-100Br	JW2-105Br	JW2-105Br*	JW2-104A-Br	JW2-104A-Br*
Trace elements						
Sc	0.9	0.5	1.2	1.6	1	0.9
Cr	51	62	570	760	540	490
Co	3.1	1.9	37	50	3.6	3.2
Ni	70±140	210	1710	2200	1820	1630
Zn	110	58	2170	2900	140	120
As	ND	ND	55	73	ND	ND
Br	11	10	25	33	35	31
Sr	3600	3100	2700	3600	3800	3400
Sb	0.8	0.4	1.6	2.1	0.9	0.8
La	98	270	200	260	310	280
Ce	240	620	410	540	830	740
Nd	250	330	290	390	660	590
Sm	54	64	56	74	0.8	0.7
Eu	9.7	12	9.8	13	27	24
Tb	6.1	8.5	6.7	8.9	18	16
Yb	1.8	7.6	2.7	3.6	7.2	6.5
Lu	0.3±0.2	0.9	0.4	0.5	0.7	0.7
Au	20±10	10±9	22	29	40±20	30±20
Th	31	31	32	42	76	68
U	2.0	22	2.4	3.2	13	11
Mass (mg)	0.11	0.34	0.07	0.09	0.05	0.05

Table 16.2 — *continued.*

China	JW2-104B-Br	JW2-103Br	JW2-103Br*	JW2-102Br	JW2-102Br*	JW2-101Br
Trace elements						
Sc	0.5	0.7	0.6	1	0.9	0.6
Cr	18	210	180	450	390	43
Co	1.8	4.6	4	7.4	6.4	1.9
Ni	110±90	660	570	1420	1230	160
Zn	150	56	49	ND	ND	ND
As	ND	ND	ND	10±5	9±5	ND
Br	42	250	210	33	29	62
Sr	2100	1700	1500	2000	1700	1400
Sb	0.5	0.8	0.7	1	0.8	0.6
La	450	290	250	520	450	320
Ce	1280	610	520	1300	1130	800
Nd	1050	340	290	840	730	550
Sm	230	70	61	160	140	95
Eu	47	12	11	26	23	17
Tb	28	8.6	7.5	22	19	11
Yb	11	8.1	7	17	15	6.4
Lu	1	0.9	0.8	2	1.8	0.6
Au	21	2±15	2±15	20±10	21	10±10
Th	61	52	45	87	75	75
U	19	48	42	21	18	27
Mass (mg)	0.32	0.18	0.16	0.23	0.20	0.31

Table 16.2 — *continued.*

China	JW2-100Br	JW2-100Br*
Trace elements		
Sc	1.1	2.1
Cr	490	910
Co	7.4	14
Ni	1520	2810
Zn	ND	ND
As	ND	ND
Br	83	150
Sr	1100	2040
Sb	1.4	2.6
La	790	1470
Ce	420	790
Nd	250	460
Sm	47	86
Eu	8.5	16
Tb	5.4	10
Yb	3.6	6.7
Lu	0.5	1
Au	52	96
Th	36	67
U	25	46
Mass (mg)	0.08	0.15

ND, not detected; NA, not analysed.

All trace-element concentrations are in parts per million, except gold which is in parts per billion.

* Weight corrected to average CaO content of 52 wt. %.

as follows: lanthanum, samarium, europium, thorium < 2%; scandium, cerium, terbium, ytterbium, lutetium < 5%; strontium, neodymium, uranium < 10%; chromium, cobalt, nickel, arsenic, zinc, bromine < 20%; antimony, gold < 30%. Where the precision is low, i.e. $1\sigma > 50\%$, the upper limit values are listed in Table 16.2 (In Figs. 16.5–16.8, these values are given a different symbol (see figure captions).) A complete listing of data including exact 1σ error has been given by Wright (1985).

16.4 BIOSTRATIGRAPHY AND CHRONOSTRATIGRAPHY

We have chosen a stratigraphic interval that has been carefully studied and constrained on the basis of conodonts and trilobites in the western USA (Miller *et al.*, 1982; Miller, 1984). Fig. 16.3 illustrates correlation of strata in Texas, Oklahoma and Utah with biostratigraphic and chronostratigraphic units. Correlation horizons are based on a combination of trilobite and conodont biostratigraphic zones and subzones currently recognized in the western USA. Not all these horizons have been identified in southeast China. The base of the *Missisquoia depressa* trilobite subzone is at present regarded as the Cambrian–Ordovician boundary in the USA. There is as yet no international agreement on the biostratigraphic position of the Cambrian–Ordovician boundary and therefore no globally accepted chronostratigraphic classification of this interval. This problem is being studied by the IUGS Working Group on the Cambrian–Ordovician Boundary. Chemical events observed as signatures in this study may be useful in redefining the position of this chronostratigraphic horizon.

In the Jiangshan area of Zhejiang Province, southeast China, the Cambrian–Ordovician boundary has been placed at the base of the *Hysterolenus* trilobite zone (Lu and Lin, 1983). We have arbitrarily used the Cambrian–Ordovician boundary as defined in each of these regions as the primary correlation horizon for all four sections. Other biostratigraphic horizons used for correlation purposes in the USA are the bases of trilobite and/or conodont zones or subzones as indicated in Fig. 16.3. The bases of the *Missisiquoia depressa* trilobite subzone and the *Missisquoia typicalis* trilobite subzone = the *Clavohamulus elongatus* conodont subzone correlate within a hiatus in the Texas section. A broken line across the hiatus in Figs. 16.4–16.8 connects the samples on either side of the erosional surface. The hiatus interval is represented by similar broken lines connecting correlative samples in the Oklahoma and Utah sections in these figures.

16.5 RESULTS AND DISCUSSION: CERIUM ANOMALY

Rare-earth elements are normalized to a well-characterized standard to remove the odd–even effect of elemental abundances. We use the North American Shale Composite Standard (Haskin *et al.*, 1968) to normalize the rare-earth elements in our samples. Then the rare-earth elements are plotted with the concentrations on a logarithmic scale versus the atomic number on a linear scale. This type of plot permits visual representation of significant variations. One of these variations is the variation in cerium relative to neighbouring elements lanthanum and neodymium. In some samples, cerium concentrations are higher (enriched) and, in other samples, cerium concentrations are lower (depleted) than lanthanum and neodymium concentrations. The cerium variation can be isolated by giving a mathematical value to its position on the line between lanthanum and neodymium, by the formula

$$\mathrm{Ce_{anom}} = \log\left(\frac{3\mathrm{Ce}_n}{2\mathrm{La}_n + \mathrm{Nd}_n}\right),$$

where n is the shale-normalized value of each rare earth (from Elderfield and Greaves, 1982). Comparison with analyses of fish debris in modern sediments from different environments shows that $\mathrm{Ce_{anom}}$ values < -0.10 indicate a

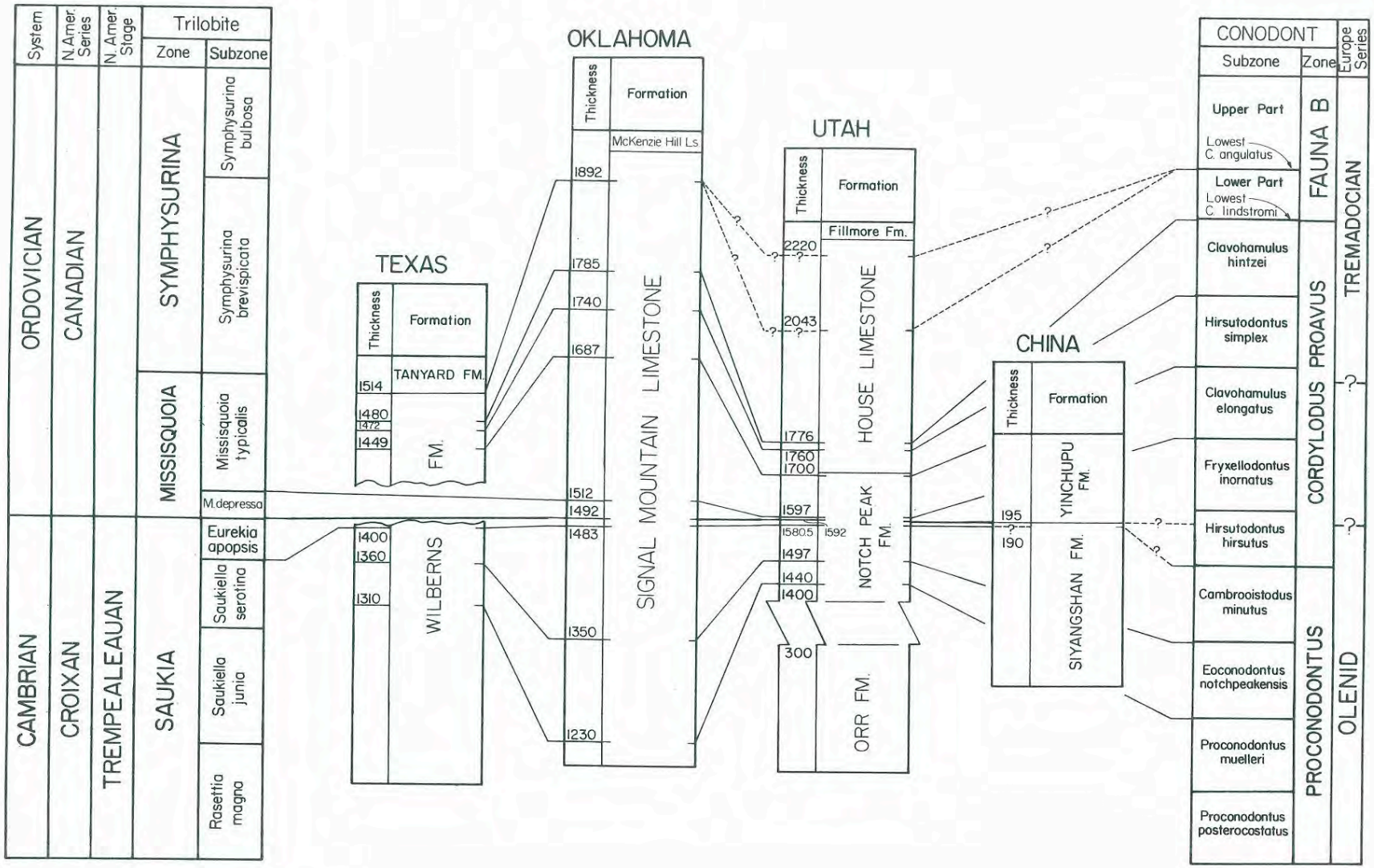

Fig. 16.3 — Correlation of strata in Texas, Oklahoma, Utah and China with biostratigraphic and chronostratigraphic units. Scale in feet as indicated for each section. Texas and Utah are composite sections. Correlation horizons are based on a combination of conodont and trilobite zones and subzones as recognized and used in the western USA. Each horizon is defined as the base of the respective zone. These same horizons are used as reference points in subsequent chemostratigraphic correlation charts.

depletion of cerium contents under suboxic to oxic conditions at the sediment–water interface or in the main water mass. Conversely, $Ce_{anom} > -0.10$ indicate enrichment of cerium under predominantly anoxic conditions (Wright, 1985; Wright *et al.*, 1985).

Fig. 16.4 shows the variations in Ce_{anom} in each section. The Cambrian–Ordovician boundary, as defined in each geographical region, is assumed to be synchronous, and the sections are 'hung' on this chronostratigraphic horizon. Additional biostratigraphic horizons are shown as full lines where known and broken lines where inferred. By using these reference horizons in USA sections, the shifts in Ce_{anom} are seen to correlate well across an interval from below the *Cordylodus proavus* Zone to above the *Missisquoia typicalis* Subzone. In the Oklahoma and Utah sections, Ce_{anom} values peak above the *C. proavus* Zone, increase between the *M. depressa* and the *M. typicalis* subzones and decrease between the *C. proavus* Zone and the *M. depressa* Subzone and above the *M. typicalis* Subzone. A lowering of the sea level and resulting period of erosion during the Lange Ranch Eustatic Event is represented by the hiatus in the Texas section (Miller, 1984). In Fig. 16.4 a broken line connects samples below and above this unconformity surface. Equivalent samples are connected by broken lines in the Oklahoma and Utah sections. Despite the erosional event, the Texas section has variations in Ce_{anom} that are similar to those observed in Oklahoma and Utah, e.g. a peak at the *C. proavus* Zone and a decrease above the *M. typicalis* Subzone.

It is important to note that the basis of the Ce_{anom} correlations are three well-constrained

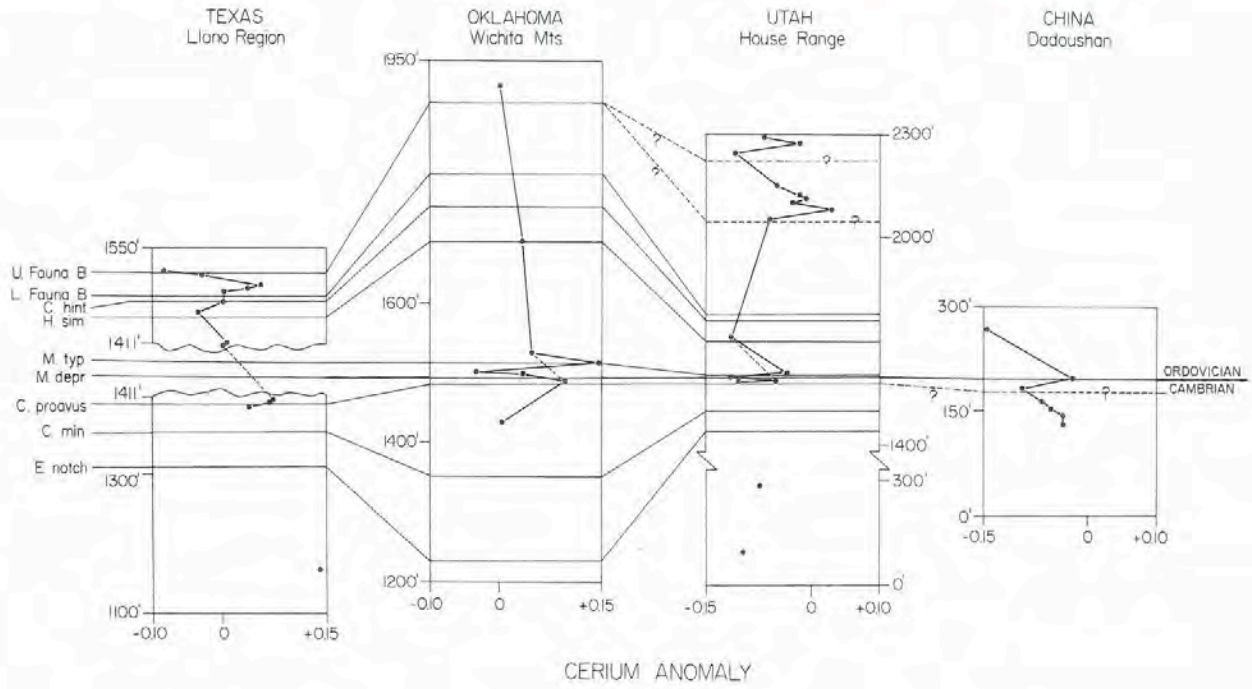

Fig. 16.4 — Correlation of Ce_{anom} in four sections. The folowing abbreviations for the correlation horizons are used in Figs. 16.4–16.8: E. notch., *Eoconodontus notchpeakensis*; C. min., *Cambrooistodus minutus*; C. proavus, *Cordylodus proavus*; M. depr., *Missisquoia depressa*; M. typ., *Missisquoia typicalis*; H. sim., *Hirsutodontus simplex*; C. hint., *Clavohamulus hintzei*; L. Fauna B, lower fauna B; U. Fauna B, upper fauna B. The broken line connects samples above and below unconformity surface in Texas and correlative samples in Oklahoma and Utah.

biostratigraphic zones that occur within a very short time interval. Using the biostratigraphic zones as tie lines between the sections, the highs and lows of Ce_{anom} values are observed to occur at the same stratigraphic position in all three western USA sections. This is even true in the Texas section where part of the interval was removed by erosion. The probability that five specific biostratigraphically constrained chemical correlations occurred by chance in three sections is extremely low.

The section from southeast China has Ce_{anom} values that are low at the inferred position of the *C. proavus* Zone and high at the *M. depressa* Subzone, which is the opposite of Ce_{anom} in the western USA. The lack of correlation of Ce_{anom} values from USA to China may be explained in several ways.

(1) The global correlation of biostratigraphic horizons *C. proavus* and *M. depressa* has not been established. When biostratigraphic studies are completed the question may be resolved by a precise placement of these horizons.

(2) If we assume that plate reconstructions in Fig. 16.1 are approximately correct, it is apparent that the USA and Chinese sections border on ocean basins that were probably not well 'connected' in terms of mixing times of surface waters (Parrish, 1982). Additionally, cerium and other rare earths have short residence times, e.g. 80 years for cerium (Schopf, 1980). Under these circumstances, heterogeneity would be reinforced so that short residence times coupled with the time necessary for mixing of surface waters between ocean basins could have prevented transmission of a chemical event.

(3) Cerium is very soluble in a water column dominated by anoxic conditions. This increased solubility could produce an overall increase in the sea-water concentration of cerium. Under dominantly anoxic conditions in the oceanic water column, the residence time of cerium would increase, so that short-term local perturbations would not effect the overall balance of cerium in the world ocean (Wright, 1985).

The base of Upper Fauna B, thought to approximate the base of the Upper Tremadoc Series in the western USA, is well defined in the Texas and Oklahoma sections, but its exact position has only been inferred in Utah. In sections in Texas and Utah the sampling interval is close enough to show significant trends that might suggest the location of this horizon. There is a very obvious spike in Ce_{anom} (Fig. 16.4) between Lower Fauna B and Upper Fauna B in Texas. A similar spike occurs in the Utah section, which suggests that the base of Upper Fauna B probably occurs near 2100 ft in the measured Utah section.

16.6 RESULTS AND DISCUSSION: OTHER TRACE ELEMENTS

Variations in concentrations of nine additional trace elements (scandium, chromium, cobalt, nickel, zinc, arsenic, antimony, thorium and gold) are plotted for each section in Figs. 16.5–16.8. Correlation horizons *E. notchpeakensis* through Upper Fauna B (from Fig. 16.3), where known, are indicated on the right-hand side of each figure. Trace-element concentrations are in parts per million, except Au, which is in parts per billion. Trace-element fluctuations may be useful in determining the positions of correlation horizons *C. proavus* or *M. depressa* in China (Fig. 16.5). For reference the eight samples analysed for the China section are numbered 1–8 from oldest to youngest on the scandium profile in Fig. 16.5. All trace-element concentrations are low in samples 7 and 8. In sample 6, seven trace elements are enriched; only thorium and gold are not. Sample 5 has higher concentration of nickel, thorium and gold, but all other trace-element contents are lower than in the previous sample. In sample 4, concentrations of all trace elements are low. Sample 3 shows an increase in trace-

element concentrations and thorium peaks here. In sample 2, only thorium concentrations remain high; all other trace elements are low. The oldest sample has high concentrations of scandium, chromium, antimony, nickel and gold. Gold concentrations reach a peak here, and scandium and antimony are at the second-highest concentration levels in the section. The greatest concentrations of trace elements, in decreasing order of enrichment, occur in samples 6, 1 and 5.

Trace-element concentrations for samples in the Texas section vary as shown in Fig. 16.6. For the correlative interval examined in the China section, only the base of the *C. proavus* Zone is present in Texas. The bases of both the *M. depressa* and the *M. typicalis* subzones are not present in the record because of a hiatus at this interval. For this portion of the section in Texas, concentrations of seven trace elements are highest in the sample just above the base of the *C. proavus* Zone; scandium and chromium are highest in the sample just below the base of the *C. proavus* Zone. Arsenic occurs in only two samples at detectable levels, just above the base of the *C. proavus* Zone and just above the erosional unconformity.

In the correlative part of the section from Oklahoma (Fig. 16.7) the greatest trace-element enrichments occur in the sample just above the base of the *C. proavus* Zone and in the sample at the base of the *M. typicalis* Subzone. The base of the *C. proavus* Zone is enriched in scandium, chromium, nickel, thorium, gold, cobalt and zinc. The first five are the highest concentrations of these elements in this part of the section. The sample below the base of the *M. typicalis* Subzone is enriched in cobalt, nickel and antimony, and is the only sample in which arsenic occurs. The sample at the base of the *M. typicalis* Subzone shows high concentrations of chromium, thorium and gold. The horizon with the greatest enrichment of trace elements is at the base of the *C. proavus* Zone.

The section from Utah (Fig. 16.8) also shows a very enriched zone of all trace elements just above the base of the *C. proavus* zone. Western USA sections consistently have the same enriched zone of trace elements just above the base of the *C. proavus* Zone. In samples from Texas and Utah, this zone also coincides with a zone of high arsenic concentration.

Tables 16.3 and 16.4 summarize the distribution of the nine trace elements in the four sections. The section from China has the greatest enrichment of trace elements at sample 6 (Table 16.3). Western USA sections (Table 16.4) show a similar enrichment at the base of *Cordylodus proavus* conodont zone which is equivalent to the *Eurekia aposis* trilobite subzone (Westrop and Ludvigsen, in press). The enrichment of trace elements at the same hori-

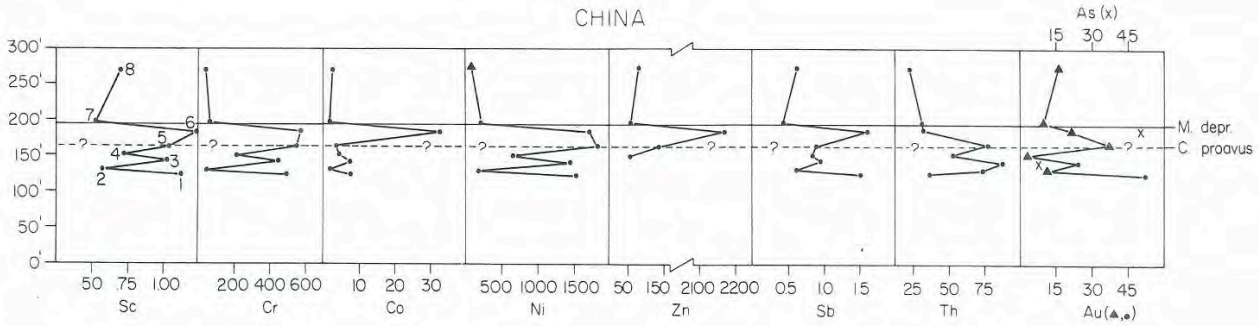

Fig. 16.5 — Variations in trace-element signatures in the China section: For explanation of abbreviations, see Fig. 16.4. In Figs. 16.5–16.8, squares are used to indicate a value with low precision (see Table 16.2 and text).

zon in the USA sections suggests that sample 6 in the section from China is the correlative horizon. Biostratigraphic study of the section from China by Miller has shown that the base of

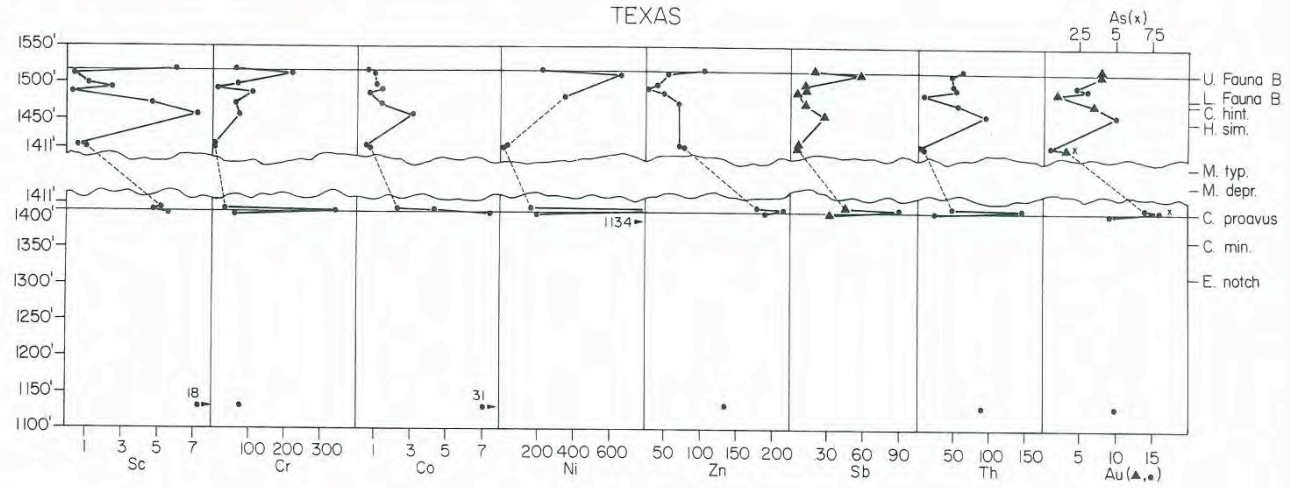

Fig. 16.6 — Variations in trace-element signatures in the Texas section. For explanation of abbreviations, see Fig. 16.4

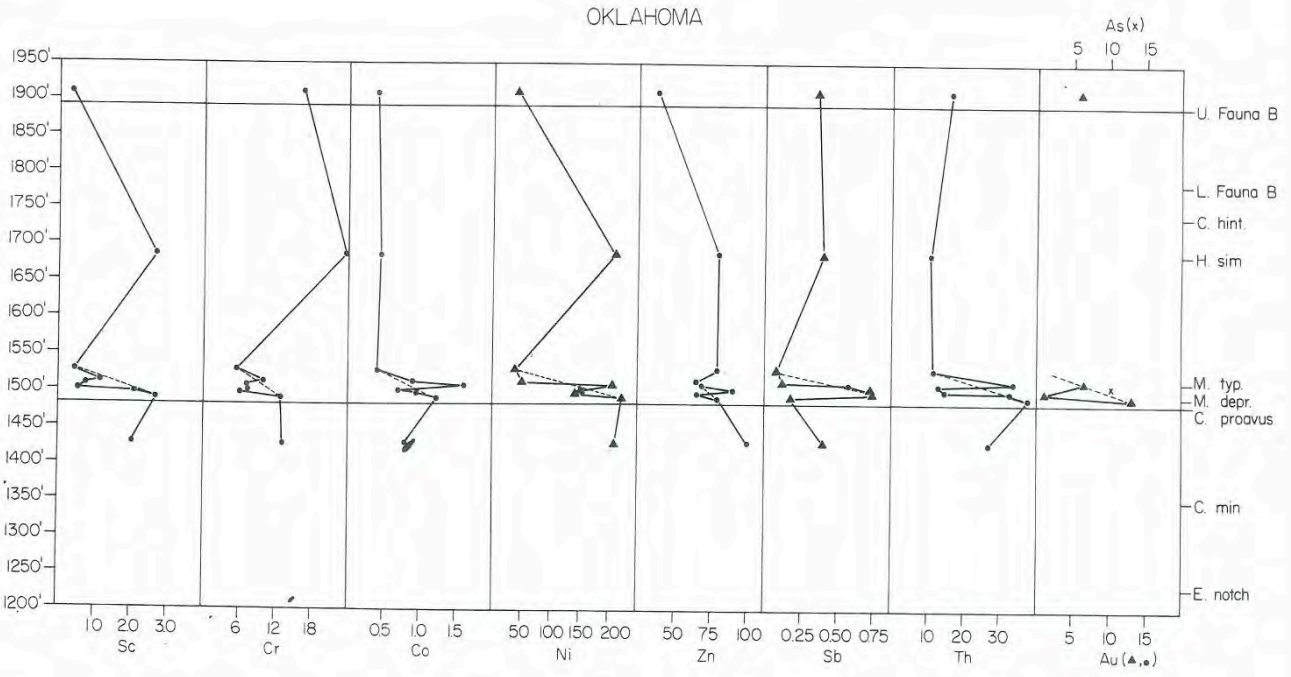

Fig. 16.7 — Variations in trace-element signatures in the Oklahoma section. For explanation of abbreviations, see Fig. 16.4

the *C. proavus* Zone in China occurs at sample 6. In this example the chemical signature predicted the location of the biostratigraphic horizon.

16.7 CONCLUSIONS

Detailed study indicates that sections at the Cambrian–Ordovician boundary interval display correlative variations in the trace-element contents of apatite of conodonts and inarticulate brachiopods. This research provides a new method of stratigraphic correlation, a method we refer to as chemostratigraphy. The use of a *group* of trace elements apparently is a reliable indicator of synchroneity in the stratigraphic record. Several lines of future research are indicated in order to establish fully the reliability of this method. First, sampling must be extended to global coverage of coeval strata to determine whether the chemical events recorded across the northern ocean also were significant in the southern hemisphere and the

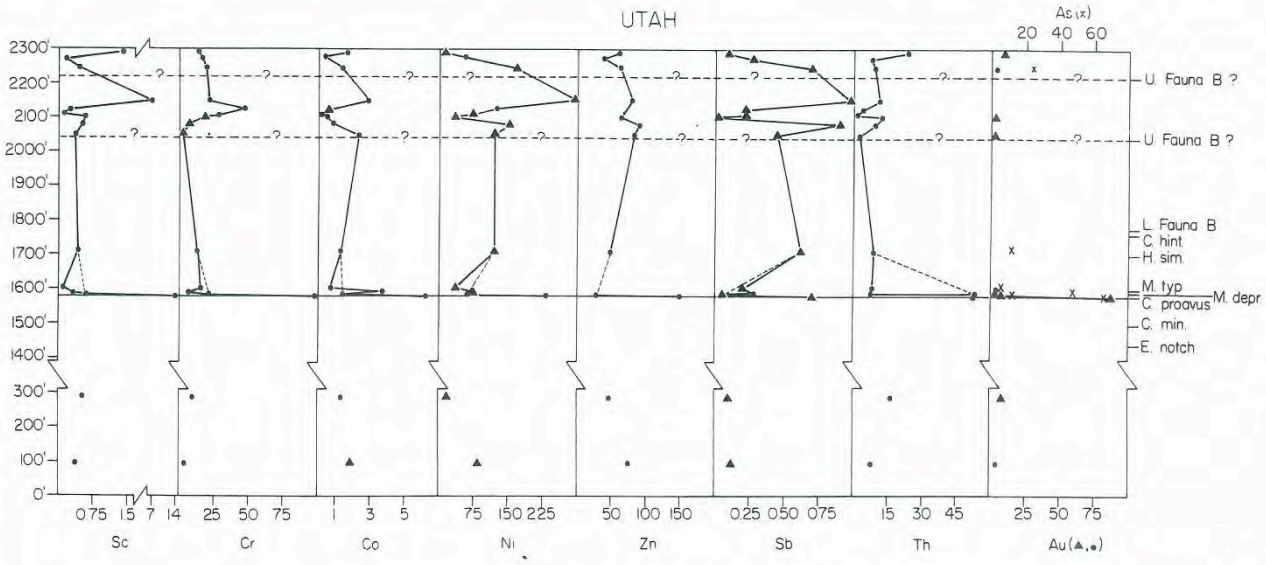

Fig. 16.8 — Variations in trace-element signatures in the Utah section. For explanation of abbreviations, see Fig. 16.4

Table 16.3 – Distribution of trace elements: China.

Sample	Sc	Cr	Co	Ni	Zn	As	Sb	Th	Au
8									
7									
6	X	X	X	X	X	X	X		
5	X	X	X					X	X
4									
3	X	X		X				X	
2								X	
1	X	X		X			X		X

X, peak in concentration level for this element.

Table 16.4 – Distribution of trace elements: western USA.

Sample	Sc	Cr	Co	Ni	Zn	As	Sb	Th	Au
Base of the *M. typicalis* Zone		O						O	O
Between			O	O	O	O	O		
Base of the *M. depressa* Zone									
Between									
Base of the *C. proavus* Zone	OU	TOU	OU	TOU	TOU	TU	TU	TOU	TOU
Below the *C. proavus* Zone	T		T						

T, peak in concentration for this element in the Texas section; O, peak in concentration for this element in the Oklahom section; U, peak in concentration for this element in the Utah section.

world ocean. Such research may resolve some of the mysteries of oceanic circulation and mixing during the Palaeozoic Era. Results of further study also may confirm that certain trace-element variations are useful only for regional correlation whereas others are valid worldwide. Second, this method must be tested at additional stratigraphic intervals where there are also sufficient biostratigraphic data to provide an independent basis for correlation of samples. These broader studies will provide a sufficient data base to model the relationships that control the chemical signals. Trace-element chemostratigraphy will eventually become a reliable tool for correlating poorly fossiliferous strata which cannot be correlated by biostratigraphic methods.

16.8 ACKNOWLEDGEMENTS

Professor Lu Yan-hao and others at the Nanjing Institute of Geology and Palaeontology, China, assisted in the field work and arranged logistical support for collecting in China. Michael E. Taylor (US Geological Survey) assisted with shipping samples from China. Tim Carr, Dell Potter (ARCO Research, Dallas) and Steve Aronoff assisted with field work in the western USA. Richard S. Seymour (EG&G Ortec, Oakridge, Tennessee), Marilyn Lindstrom and Randy L. Korotev (Washington University, St. Louis, Missouri) were instrumental in the development and adaptation of instrumental neutron activation analysis procedures for the analysis of low-mass fossil material. We thank Richard J. Williams and Douglas P. Blanchard for providing laboratory facilities and irradiation costs at the Johnson Space Center, National Aeronautics and Space Administration. Ann Wright patiently typed and edited different versions of the manuscript. This research was supported by the National Science Foundation (Grants EAR 83-19429,EAR 81-15985 and EAR 78-21819 (Holser and Wright) and EAR 81-08621 (Miller)). This research represents part of the senior author's Ph.D. dissertation at the University of Oregon, Eugene.

16.9 REFERENCES

Budge, D. R. and Sheehan, P. M. 1980. The Upper Ordovician through Middle Silurian of the eastern Great Basin: Part 1, Introduction, historical perspective and stratigraphic synthesis. *Milwaukee Public Museum Contributions in Biology and Geology*, **28**, 1–26.

Deer, W. A., Howie, R. A. and Zussman, J. 1966. *An*

Introduction to the Rock Forming Minerals, Longman, London, 504–509.

Elderfield, H. and Greaves, M. J. 1982. The rare earth elements in sea water. *Nature,* **296**, 214–219.

Elderfield, H. and Pagett, R. In press. REE in ichthyoliths: variations with redox conditions and depositional environment. In J. P. Riley (Ed.), *The Science of the Total Environment.*

Haskin, L. A., Haskin, M. A., Frey, F. A. and Wildeman, T. R. 1968. Relative and absolute terrestrial abundance of the rare earths. In L. H. Ahrens (ed.), *Origin and Distribution of the Elements, Vol. 30,* Pergamon Press, London, 889–912.

Hintze, L. F. 1982. Ibexian Series (Lower Ordovician) type section, western Utah, USA. In R. J. Ross, Jr. and S. M. Bergström (Eds.), *The Ordovician System in the United States, Correlation Chart and Explanatory Notes, International Union of Geological Sciences,* **12**, 7–10.

Jacobs, J. W., Korotev, R. L., Blanchard, D. P. and Haskin, L. A. 1977. A well-tested procedure for instrumental activation analysis of silicate rocks and minerals. *Journal of Radioanalytical Chemistry,* **40**, 93–114.

Keto, L. S. and Jacobson, S. B. 1985. Implications for paleo-oceanography from Nd and Sr isotope ratios of Lower Paleozoic brachiopods. *EOS Transactions, American Geophysical Union,* **66**, (18), 424.

Korotov, R. L. In press. National Bureau of Standards coal fly ash (SRM-1633A) as a multielement standard for instrumental neutron activation analysis. *Journal of Radioanalytical and Nuclear Chemistry.*

Laul, J. C. 1979. Neutron activation analysis of geological materials. *Atomic Energy Reviews,* **17**, 603–695.

LeMone, D. V. 1975. Correlation aspects of the Ordovician of the southwestern United States. In J. M. Hills (Ed.), *Exploration from the Mountains to the Basin,* El Paso Geological Society, 1975 Guidebook, El Paso, Texas, 169–190.

Lindstrom, D. J. and Korotev, R. L. 1982. TEABAGS: computer programs for instrumental neutron activation analysis. *Journal of Radioanalytical Chemistry,* **70**, 439–458.

Lu, Y.-H. and Lin, H.-L. 1983. Uppermost Cambrian and lowermost Ordovician trilobites of Jiangshan–Changshan area. In *Papers for the Symposium on the Cambrian–Ordovician and Ordovician–Silurian Boundaries,* Nanjing Institute of Geology and Palaeontology, Academia Sinica, 6–11.

Miller, J. F. 1984. Cambrian and earliest Ordovician conodont evolution, biofacies and provincialism. In D. L. Clark (Ed.), *Conodont Biofacies and Provincialism, Geological Society of America Special Paper,* **196**, 43–68.

Miller, J. F., Taylor, M. E., Stitt, J. H., Ethington, R. L. Hintze, L. F. and Taylor, J. F. 1982. Potential Cambrian–Ordovician boundary stratotype sections in the western United States. In M. G. Bassett and W. T. Dean (Eds.), *The Cambrian-Ordovician Boundary: Sections, Fossil Distributions and Correlations, Geological Series 3,* National Museum of Wales, Cardiff, 155–180.

Parrish, J. T. 1982. Upwelling and petroleum source beds, with reference to Paleozoic. *American Association of Petroleum Geologists Bulletin,* **66**, 750–774.

Pietzner, H., Vahl, J., Werner, H. and Ziegler, W. 1968. Zur chemischen Zusammensetzung und Mikromophologie der Conodonten. *Palaeontographica,* **128**, 115–152.

Schopf, T. J. M. 1980. *Paleoceanography,* Harvard University Press, Cambridge, Massachusetts, 151.

Scotese, C. R., Bambach, R. K., Barton, C., Van Der Voo, R. and Ziegler, A. M. 1979. Paleozoic base maps. *Journal of Geology,* **87**, 240, Fig. 6.

Shaw, H. F. 1984. Sm–Nd and Rb–Sr systematics of tektites and other impactites, Appalachian mafic rocks, and marine carbonates and phosphates. *Ph.D. Dissertation,* California Institute of Technology, Pasadena, California, 1–282.

Shaw, H. F. and Wasserburg, G. J. 1985. Sm–Nd in marine carbonates and phosphates: implications for Nd isotopes in seawater and crustal ages. *Geochimica et Cosmochimica Acta,* **49**, 503–518.

Staudigel, H., Doyle, P. and Zindler, A. In press. Sr and Nd isotope systematics in fish teeth. *Earth and Planetary Science Letters.*

Westrop, S. R. and Ludvigsen, R. In press. Type species of the basal Ibexian trilobite *Corbinia* Walcott. *Journal of Paleontology.*

Wright-Clark, J. 1982. The geochemistry of conodont apatite: secular variations inferred by comparison with the cerium–iron system in the modern ocean. *Unpublished M.Sc Thesis,* University of Oregon, Eugene, Oregon, 1–67.

Wright, J. 1985. Rare earth element distributions in Recent and fossil apatite: implications for paleoceanography and stratigraphy. *Ph.D. Dissertation* University of Oregon, Eugene, Oregon, 1–259.

Wright, J. and Holser, W. T. 1981. Rare earth elements in conodont apatite as a measure of redox conditions in ancient seas. *Geological Society of America Abstracts,* **13**, 586.

Wright, J., Seymour, R. S. and Shaw, H. F. 1984. REE and Nd isotopes in conodont apatite: variations with geological age and depositional environment. In D. L. Clark (Ed.), *Conodont Biofacies and Provincialism, Geological Society of America Special Paper,* **196**, 325–340.

Wright, J., Schrader, H. and Holser, W. T. 1985. Paleoredox of seawater from cerium variations in fossil apatite. *Geological Society of America Abstracts,* **17**, 755.